IEICE Electronics Express, Vol.17, No.11, 1–6

LETTER

Direct synthesis of slot arrays for 5G communication applications

Chunmei Liu[1], **Wen Cao**[1], **Xin Cao**[1, a)], **and Weiping Li**[2]

Abstract In this paper, a slot array in 5G communication band is proposed. The pattern function is first modified and calculated. Then, the array is constructed using rectangular waveguides. Based on our simulated and measured results, the proposed method has successfully achieved the slot arrays with low side lobes and high gain. The proposed antenna arrays can be applied in modern 5G communication systems.

Keywords: antenna arrays, slot antenna, rectangular waveguide, 5G communication

Classification: Microwave and millimeter-wave devices, circuits, and modules

1. Introduction

Slot antennas have a wide range of applications and the aperture distribution of a waveguide slot array antenna can be independently controlled [1, 2, 3, 4, 5, 6]. By controlling the amplitude distribution and phase distribution of its aperture surface, it is relatively easy to achieve low or extremely low side lobes [7, 8, 9, 10, 11]. Beam forming techniques are attractive in modern 5G microwave communications and radar system designs [12, 13, 14, 15, 16]. Waveguide slot antenna arrays are highly valued for their compact structure, good mechanical strength, high radiation efficiency, low feed loss, large power capacity, and high reliability [17, 18, 19, 20, 21, 22, 23]. Waveguide slot antenna has many advantages. The waveguide slot antenna is relatively easy to control the aperture distribution, and there is no energy loss caused by the irradiation of the feed source, nor does it affect the observation range because of the aperture shielding, and it does not have the defect of a high level of far side lobes [24, 25, 26, 27, 28]. 5G communications systems in the millimeter regions are given in Table I, where it is divided into five sub-bands named from n257–n261 [29]. In this paper, a method for designing the aperture distribution of a waveguide slot array antenna is proposed, and a comprehensive design of the array antenna is completed. The synthesis principle of synthesis method is introduced, and the advantages and disadvantages of Taylor or Chebyshev are compared; circle caliber synthesis method, circular caliber continuous excitation distribution, and circular caliber rectangular grid excitation are analyzed. According to the antenna design specifications, a circular array distribution is used to synthesize the radiation pattern to obtain the original aperture rectangular grid excitation level distribution of the waveguide slot array antenna, and then the waveguide slot array is used to approximate the aperture excitation level distribution.

Table I 5G operating bands in millimeter wave regions

Sub-bands	Uplink or Downlink Operating Bands		Duplex mode
	Frequency range (GHz)	Bandwidth (GHz)	
n257	26.5-29.5	3	TDD
n258	24.25-27.5	3.25	TDD
n259	39.5-43.5	4	TDD
n260	37-40	3	TDD
n261	27.5-28.35	0.85	TDD

The aim of the proposed method is to take quantization effect into account. The circular is discretized by the slot units, and with the proposed method, we can determine whether to take or leave the slots on the edge in order to achieve the highest gain with the lowest sidelobes. The problem with Chebyshev method is that the sidelobes at the ±90° of the mainlobe are relatively high. The problem with Taylor method is that the sidelobes near the mainlobe are relatively high. Therefore, in both methods, the sidelobes may not be effectively suppressed and therefore the gain of the antenna array can be compromised.

The designed frequency of the antenna array is at 28 GHz, which can be applied in the n257 and n261 sub-bands of the 5G communication systems.

2. Theory and design process

2.1 Synthesis process

The antenna elements can be any type of radiating antenna, but the type of the radiating elements in the same array antenna must be the same, and the form of array elements in space is also the same. According to the arrangement of array elements in space, a variety of array antennas such as one-dimensional linear array, two-dimensional planar array, and three-dimensional spatial array can be formed. The radiation characteristics of an array antenna mainly depend on the type, number, and arrangement of the array elements, the cell spacing, and the amplitude and phase distribution of the excitation current on each cell. The design of the array antenna first requires proper array synthesis, that is, the radiation pattern is synthesized under the condition that the

[1] School of Information Engineering, Southwest University of Science and Technology, Mianyang, China
[2] School of Information Engineering, East China Jiaotong University, Nanchang, China
[a)] caoxin@swust.edu.cn

DOI: 10.1587/elex.17.20200135
Received April 7, 2020
Accepted May 7, 2020
Publicized May 26, 2020
Copyedited June 10, 2020

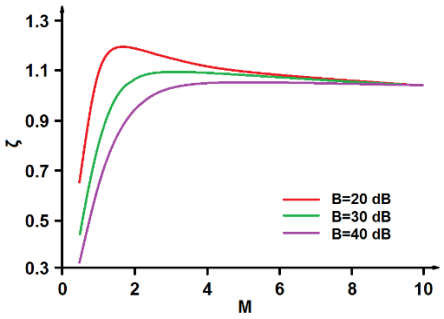

Fig. 1 The graph of lobe broadening factors ζ and M

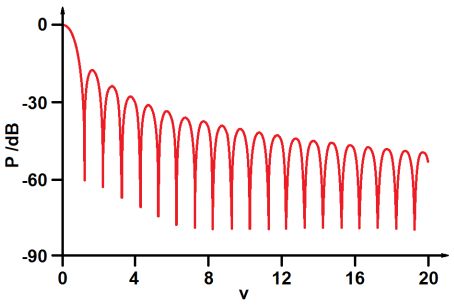

Fig. 2 The normalized pattern function

required radiation characteristics are met, and the array pattern shape, main lobe width, sidelobe level, and directivity are obtained. Coefficient, from which the number of cells in the array, cell spacing, excitation amplitude, and phase distribution are obtained.

For line array, the pattern function can be expressed as [30]

$$P(u) = \cosh(\pi B)\frac{\sin(\pi v)}{\pi v} \tag{1}$$

Since the side lobe level of the basic function $\sin(\pi v)/(\pi v)$ is relatively high, a new line source pattern function is built based on the principle that moving the zero position to the far sidelobe direction can reduce the side lobe level.

$$P(u) = \cosh(\pi B)\frac{\sin(\pi v)}{\pi v}\frac{\prod_{m=1}^{M-1}\left[1-(v/v_m)^2\right]}{\prod_{m=1}^{M-1}\left[1-(v/m)^2\right]} \tag{2}$$

The significance of this pattern function is to replace the previous zero point of the basic function with the zero point of the rewritten ideal space factor, and the zero point after the first zero point is still the zero point of the original basic function. Then the zero position becomes

$$v_n = \begin{cases} \pm\varsigma\sqrt{B^2+(m-1/2)^2}, & 1 \le m \le M-1 \\ \pm m, & M \le m \le \infty \end{cases} \tag{3}$$

Function (3) is continuous in the defining range, then we have

$$\varsigma = \frac{M}{\sqrt{A^2+(M-1/2)^2}} \tag{4}$$

The relation between ζ and M has been plotted in Figure 1 with different values of B.

Since

$$\frac{\sin(\pi v)}{\pi v} = \prod_{m=1}^{\infty}\left[1-\left(\frac{v}{m}\right)^2\right] \tag{5}$$

then we have

$$P(v) = \cosh(\pi B)\prod_{m=M}^{\infty}\left[1-(v/m)^2\right]\cdot\prod_{m=1}^{M-1}\left[1-(v/v_m)^2\right] \tag{6}$$

Circular aperture pattern with respect to θ can be given as

$$P(\theta) = 2\pi a^2\frac{J_1(ka\sin\theta)}{ka\sin\theta} \tag{7}$$

where a is the radius of the aperture, J_1 is the Bessel function. The normalized pattern function is

$$P(v) = 2\frac{J_1(\pi v)}{\pi v} \tag{8}$$

where

$$v = \frac{2a}{\lambda}\sin\theta \tag{9}$$

The normalized pattern function has been plotted in Figure 2.

Since the space factor $P(\theta)$ is axisymmetric, the stereo pattern can be obtained by rotating the graph in Figure 2 around the z-axis. The main lobe beam is conical, and the side lobe level is high. The far side lobe decreases exponentially. The zero position of the pattern is $\alpha_{1\mathrm{m}}$, which satisfies $J_1(\pi\alpha_{1m}) = 0$, $\mathrm{m} = 0,1,2,\ldots,m$. It is true except for $m = 0$, because $\alpha_{10} = 0$ is the position where the maximum spatial factor is located. If the side lobe is to be reduced and the level of the side lobe is adjustable, a new circular aperture space factor must be constructed. Using the uniformly distributed circular aperture normalized space factor $P(v) = 2J_1(\pi v)/(\pi v)$ as the basic function of the space factor, we can remove the first zero point $\alpha 1\mathrm{m}$ next to the main lobe, and use them as new zero point. These new zero points should meet two conditions: first, there is a certain outward movement relative to the corresponding original zero position; second, the new zero position can be adjusted, so that the side lobe level can be adjusted. The new zero that satisfies these two conditions should be the zero of the modified ideal line source space factor. It can be deduced from this space factor is

$$P(u) = \cosh(\pi B)\frac{J_1(\pi v)}{\pi v}\frac{\prod_{m=1}^{M-1}\left[1-\left(\frac{v}{v_m}\right)^2\right]}{\prod_{m=1}^{M-1}\left[1-\left(\frac{v}{\alpha_{1m}}\right)^2\right]} \tag{10}$$

For rectangular grids with rectangular borders, the product of the patterns of two orthogonal linear arrays is equal to the pattern of a planar array. The principle and method of the array can be directly applied. The disadvantage of the separable distribution is that the gain is limited, but the central axis symmetrical pattern can overcome this disadvantage. Therefore, we extend line source analysis theory to a circular boundary plane array with a central axis symmetrical distribution. In this way, we only need to sample the circular distribution to obtain the excitation coefficient of the rectangular grid discrete array.

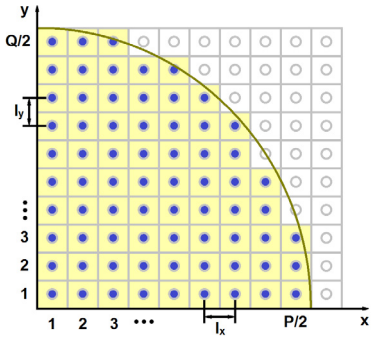

Fig. 3 Rectangular grid circular array

Let us suppose there is an $M \times N$ rectangular grid array placed in the xy plane, as shown in Figure 3. The row and column spacing are l_x and l_y, respectively. The corners are cut to form a circle plane array distribution. The coordinate of the unit (x_m, y_n) can be given as

$$\begin{cases} x_m = (m-1/2)l_x, & m = 1,2,\cdots,M/2 \\ y_n = (n-1/2)l_y, & n = 1,2,\cdots,N/2 \end{cases} \tag{11}$$

So we can get the pattern function as

$$P(\theta,\varphi) = 4\sum_{m=1}^{M/2}\sum_{n=1}^{N/2} I_{mn}(\chi_{mn}) \cos\left[\frac{(2m-1)v_x}{2}\right] \cos\left[\frac{(2n-1)v_y}{2}\right] \tag{12}$$

where

$$\begin{cases} v_x = kl_x \sin\theta\cos\varphi \\ v_y = kl_y \sin\theta\cos\varphi \end{cases} \tag{13}$$

$$\chi_{mn} = \left\{\left[\frac{(2m-1)}{2}l_x\right]^2 + \left[\frac{(2n-1)}{2}l_y\right]^2\right\}^{1/2} \tag{14}$$

Considering that the discontinuity in the waveguide excites electromagnetic waves of higher order modes, the standard waveguide WR28 is selected as the radiation waveguide to design the radiation surface of the array antenna to suppress higher modes. Assume that the common wall between the radiating waveguides is 1 mm, so the waveguide wavelength at the center frequency of the electromagnetic waves transmitted in the radiating waveguide can be obtained. Assuming that the longitudinal direction of the radiating waveguide is the x-axis, the array can be determined in the x-direction according to the principle of electromagnetic field transmission in the waveguide. The radiation pattern can be synthesized according to the index parameters by using the previously described round aperture rectangular grid array synthesis method.

When the array radius is selected as $a = 50$ mm and the number of equal side lobe levels $n = 4$, the main side lobe level ratio $R_0 = 30$ dB. The synthesized pattern using the proposed method in comparison with Chebyshev and Taylor methods is shown Figure 4. We can see that the pattern using Chebyshev method has high sidelobs at the ±90° direction, while the pattern using Taylor method has high sidelobs near the mainlobe. By comparison, the proposed method has achieved the optimal results in the whole range. Since more

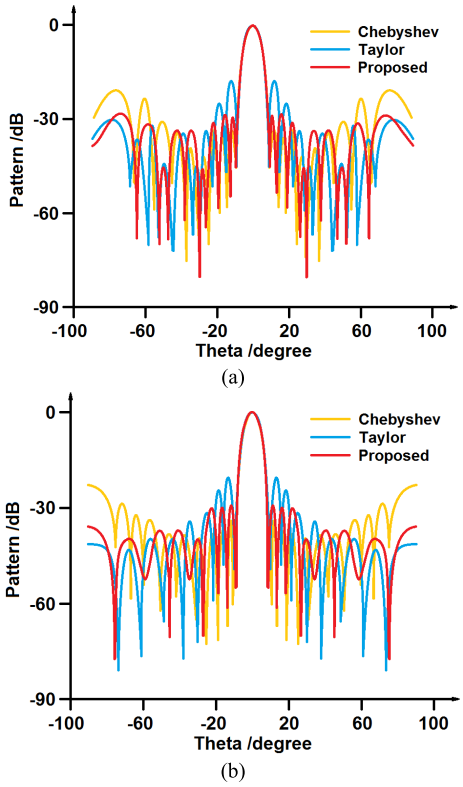

Fig. 4 The synthesized radiation pattern in the (a) E-plane and (b) H-plane in comparison with conventional methods

electromagnetic power is diverted to sidelobes in Chebyshev or Taylor method, the gain is lowered compared with the proposed method.

2.2 Waveguide and slot analysis

Based on the circular aperture synthesis method, starting from the continuous surface source current on the circular aperture, the corresponding continuous surface source excitation distribution can obtained. Then the sampling theorem is used to synthesize the required pattern, and the excitation amplitude of the discrete circular aperture array unit is obtained by sampling. The distribution of the normalized equivalent excitation current of the radiating element on the radiating surface is shown in Figure 5. We can see that the closer to the center of the array is, the higher the equivalent normalized excitation current is. It can be observed that the excitation current distribution on a single waveguide changes relatively smoothly, and the excitation amplitude at the end and the excitation amplitude of the adjacent unit becomes much smaller. As the longitudinal waveguide of the x-axis moves away from the x-axis, the number of radiating elements on the radiating waveguide gradually decreases, which is precisely to meet the circular distribution of the array antenna.

From this, we can start from the excitation amplitude distribution of the discrete circular aperture array unit of the radiation front, and obtain the normalized admittance distribution of the radiation front gap, as shown in Figure 6. It can be seen from the figure that the sum of the equivalent conductance values of the slots on each waveguide is unit, and this is because the equivalent conductance values

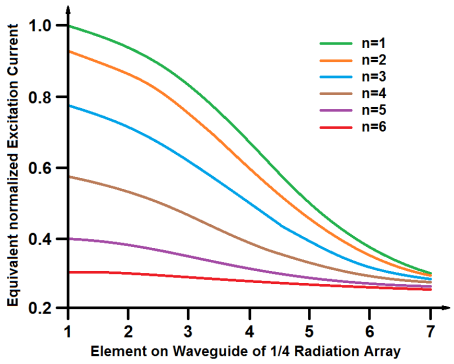

Fig. 5 The equivalent normalized excitation current of the radiation array

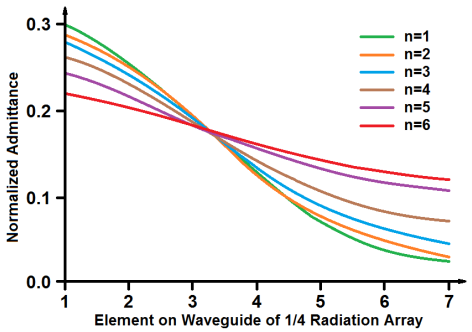

Fig. 6 The normalized admittance of the radiation gap of 1/4 radiation array

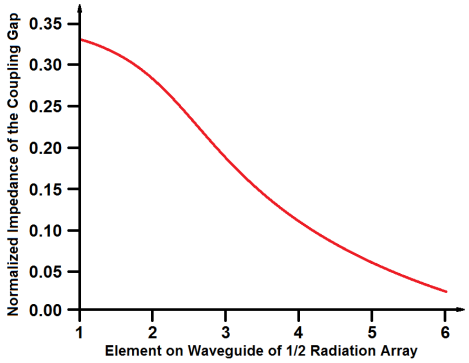

Fig. 7 The equivalent impedance of coupling gap on 1/2 radiation front

of only half of the slots of the waveguide are drawn on the figure, and the other side of the slots is equivalent. The effective conductance value is symmetrically distributed with this side.

The equivalent impedance value of the central coupling slot feeding the radiating waveguide is generally different at different positions. This is because the feeding of the center coupling slot to the radiating waveguide is determined by comprehensively considering the ratio of the energy radiated on the corresponding radiating waveguide to the total radiant energy of the array. At the same time, the form of center feeding for the coupling waveguide is considered. Figure 7 shows the equivalent resistance of the center coupling slot on the 1/2 array of the array antenna after calculation.

2.3 Simulation and measurement

The excitation amplitude distribution of the circular aperture array unit and the equivalent conductance value distribution

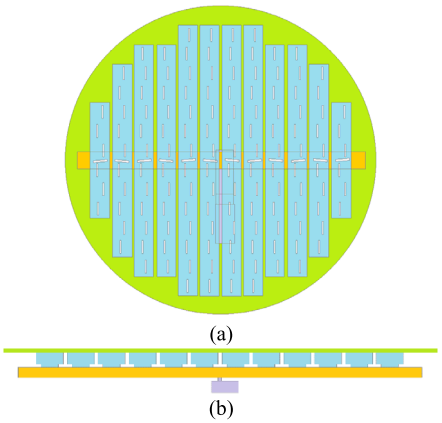

Fig. 8 The structure of the antenna array (a) top view (b) side view

of the longitudinal waveguide slot of the radiating element and the equivalent resistance value distribution of the center coupling slot have been obtained before. The standard WR28 waveguide (7.11 mm × 3.56 mm) has been chosen as the radiating waveguide, and the common wall thickness between the waveguides is 1 mm. The coupling waveguide size is 6.7 mm × 3.4 mm. All radiating waveguides are fed in-phase.

The excitation amplitude distribution of the circular aperture array unit and the corresponding longitudinal waveguide of the radiating unit have been extracted. The gap's equivalent conductance value distribution value corresponds to the extracted equivalent admittance parameters, and determines the size and offset of each radiating gap unit. A radiation front model was established. The impedance value distribution corresponds to the extracted equivalent impedance parameters, and the size and rotation angle of each coupling gap unit are determined. Based on the model of the radiation front, a model of the coupling waveguide and the coupling gap is also established. For the establishment of the excitation slot and the waveguide, the factors of the standing wave bandwidth and phase bandwidth of each coupling slot unit in the coupled waveguide must be considered comprehensively. The selection of the waveguide slot to feed the coupled waveguide is the result of comprehensive consideration. The excitation slot is a wide-border lateral slot of the waveguide with respect to the coupled waveguide, while the excitation slot is a wide-border longitudinal slot of the waveguide relative to the excited waveguide. Because the interface of the antenna is the standard WR28 waveguide interface, adding a waveguide at the end will transition the size of the excitation waveguide to the WR28 waveguide, as shown in figure 8.

Figure 9 shows the radiation patterns of the E and H planes at the center frequency at 28 GHz. From the radiation pattern of the known plane, the side lobe level of the H plane radiation pattern is 23 dB, with the 3 dB lobe width of 7°. The side lobe level of the E plane radiation pattern is 22 dB, with the 3 dB lobe width of 7°. Then, the antenna gain is over 22 dB.

The simulated voltage standing wave ratio (VSWR) is given in Figure 10. The VSWR is 1.05 at the operating frequency of 28 GHz, which means the input signal has been absorbed by the antenna with almost no reflection.

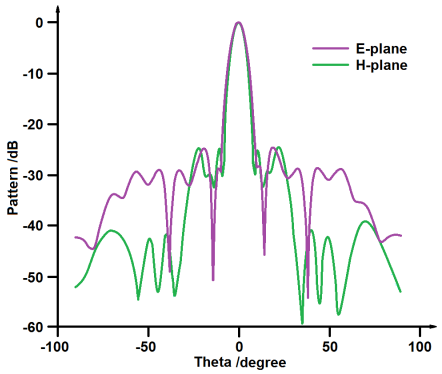

Fig. 9 The simulated E- and H-plane radiation patterns

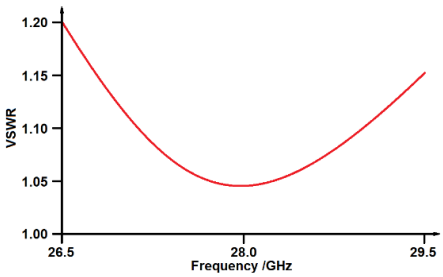

Fig. 10 The simulated VSWR of the slot-array

The antenna is fabricated after simulation. Because this antenna has an internal cavity structure, flat-plate high-speed milling is used. The radiation waveguide is too thin for the isolation of the radiation waveguides only by screw connection. Therefore, the radiation waveguide grooves are seamlessly welded, and the remaining parts are mechanically tightly connected by screws. The actual photo after the antenna is processed is shown in the figure below.

Figure 11 shows the radiation patterns of the E-plane and H-plane at 28 GHz. The figure shows that the side-lobe level of the H-plane of the radiation pattern is 27 dB with the 3 dB lobe width of 7°; The side lobe level of the E-plane of the pattern is 18 dB, and the 3 dB lobe width is 6°. The gain of the antenna is over 18 dB. It can been seen that the simulated and measured results are in good agreement. The difference between the actual test results and the simulation results is mainly due to the difference between the actual size of the array antenna and the theoretical value due to the introduction of processing errors.

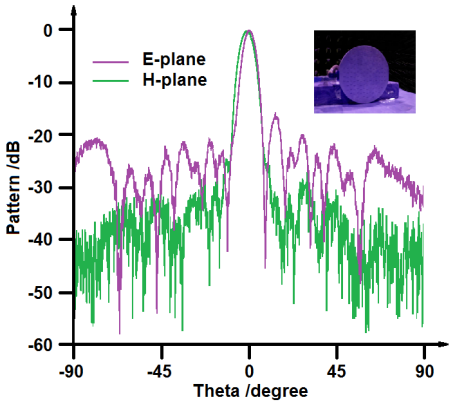

Fig. 11 The measured E- and H-plane radiation patterns

3. Conclusion

In this paper, a slot array is synthesized for 5G communication systems. The proposed method is theoretically analyzed, simulated, fabricated and measured. The measured results are in good agreement with the simulated results. The proposed antenna can be applied in n257 and n261 subbands in the 5G millimeter wave communication systems.

Acknowledgments

This work was supported by Science and Technology Research Project of Educational Commission of Jiangxi Province of China (GJJ180313).

References

[1] D. Zarifi and A. Ahmadi: "A broadband slant polarized cavity backed microstrip-fed wide-slot antenna array," Int. J. RF Microw. Comput.-Aided Eng. (2020) e22164 (DOI: 10.1002/mmce.22164).

[2] M. Li, *et al.*: "A miniaturized dual-band dual-polarized band-notched slot antenna array with high isolation for base station applications," IEEE Trans. Antennas Propag. **69** (2019) 795 (DOI: 10.1109/TAP.2019.2940471).

[3] H. Khalil, *et al.*: "Nose-cone conformal substrate-integrated waveguide slot array antenna for X-band radar applications," Int. J. Antennas Propag. **2019** (2019) 6262574 (DOI: 10.1155/2019/6262574).

[4] Y. Zong, *et al.*: "An improved dual-band shared aperture waveguide slot array antenna," Microw. Opt. Technol. Lett. **61** (2019) 2477 (DOI: 10.1002/mop.31921).

[5] D. Huang, *et al.*: "Slot antenna array for fifth generation metal frame mobile phone applications," Int. J. RF Microw. Comput.-Aided Eng. **29** (2019) e21841 (DOI: 10.1002/mmce.21841).

[6] P. Pinho and N. Carvalho: "Evaluation of planar elliptical antenna array with inner counter-elliptical slot," Radioengineering **27** (2017) 937 (DOI: 10.13164/re.2018.0937).

[7] J. Tak, *et al.*: "A 3-D-printed W-band slotted waveguide array antenna optimized using machine learning," IEEE Antennas Wireless Propag. Lett. **17** (2018) 2008 (DOI: 10.1109/LAWP.2018.2857807).

[8] M. Alibakhshikenari, *et al.*: "Antenna mutual coupling suppression over wideband using embedded periphery slot for antenna arrays," Electronics **7** (2018) 198 (DOI: 10.3390/electronics7090198).

[9] A.K. Sahoo, *et al.*: "Slot antenna array with integrated filter for WLAN application at 5.2 GHz," Wireless Personal Communications **101** (2018) 931 (DOI: 10.1007/s11277-018-5734-1).

[10] Y. Cai, *et al.*: "A 16-element corporate-feed multilayer SIW cavity-backed slot antenna array," IET Microw. Antennas Propag. **11** (2017) 1796 (DOI: 10.1049/iet-map.2016.1078).

[11] B. Cao, *et al.*: "W-band high-gain TE_{220}-mode slot antenna array with gap waveguide feeding network," IEEE Antennas Wireless Propag. Lett. **15** (2015) 988 (DOI: 10.1109/LAWP.2015.2489721).

[12] B. Bahreini, *et al.*: "Optimum design of a beam-forming array of S-shaped DRA elements with a superstrate on an SIW feed for 5G mobile systems," IEEE Antennas Wireless Propag. Lett. **18** (2019) 1410 (DOI: 10.1109/LAWP.2019.2918154).

[13] Y. Xiao, *et al.*: "Integrated resource optimization with WDM-based fronthaul for multicast-service beam-forming in massive MIMO-enabled 5G networks," Photon. Netw. Commun. **37** (2019) 349 (DOI: 10.1007/s11107-018-00821-z).

[14] K.H. Moussa and S.E. El-Khamy: "A projected fast ISTA algorithm for joint beam forming and antenna selection in massive MIMO," Wireless Networks (2018) 1 (DOI: 10.1007/s11276-018-1786-0).

[15] H. Li, *et al.*: "Wideband transparent beam-forming metadevice with amplitude- and phase-controlled metasurface," Phys. Rev. Appl. **11** (2019) 014043 (DOI: 10.1103/PhysRevApplied.11.014043).

[16] Z.W. Shan and R.K.L. Su: "Improved uncoupled closed-form solution

for adhesive stresses in plated beams based on Timoshenko beam theory," Int. J. Adhesion Adhesives **96** (2020) 102472 (DOI: 10.1016/j.ijadhadh.2019.102472).
[17] M. Fallah and M. Khalaj-Amirhosseini: "Meta-waveguide analysis and implementation for using as a slot array antenna," Int. J. Microw. Wireless Technol. **12** (2020) 138 (DOI: 10.1017/S1759078719001132).
[18] H. Medkour, *et al.*: "Coplanar waveguide-based ultra-wide band antenna with switchable filtering of WiMAX 3.5 GHz and WLAN 5 GHz signals," Microw. Opt. Technol. Lett. (2020) (DOI: 10.1002/mop.32321).
[19] Z. Gholipour and J. Ahmadi-Shokouh: "Substrate integrated waveguide corrugated horn antenna," Wireless Personal Communications **109** (2019) 1605 (DOI: 10.1007/s11277-019-06640-3).
[20] Y. Ji, *et al.*: "Reconfigurable phased-array antenna using continuously tunable substrate integrated waveguide phase shifter," IEEE Trans. Antennas Propag. **67** (2019) 6894 (DOI: 10.1109/TAP.2019.2927813).
[21] N.K. Mungaru, *et al.*: "A quad-band Sierpenski based fractal antenna fed by co-planar waveguide," Microw. Opt. Technol. Lett. **62** (2020) 893 (DOI: 10.1002/mop.32097).
[22] N. Wang and X. Xu: "A compact planar circularly polarized eighth-mode substrate integrated waveguide antenna," Int. J. Microw. Wireless Technol. **10** (2018) 956 (DOI: 10.1017/S175907871800051X).
[23] S.-P. Gao, *et al.*: "Equivalent model built with limited information: predicting installed performance of slotted waveguide antennas," IEEE Antennas Propag. Mag. **60** (2018) 52 (DOI: 10.1109/MAP.2018.2859163).
[24] M.M. Sabahi, *et al.*: "A compact CRLH circularly polarized leaky-wave antenna based on substrate-integrated waveguide," IEEE Trans. Antennas Propag. **66** (2018) 4407 (DOI: 10.1109/TAP.2018.2851278).
[25] A. Zhang, *et al.*: "Metasurface-based tapered waveguide slot array antennas for wide angular scanning in a narrow frequency band," IEEE Trans. Antennas Propag. **66** (2018) 4052 (DOI: 10.1109/TAP.2018.2839902).
[26] P. Sanchez-Olivares, *et al.*: "Mechanically reconfigurable linear array antenna fed by a tunable corporate waveguide network with tuning screws," IEEE Antennas Wireless Propag. Lett. **17** (2018) 1430 (DOI: 10.1109/LAWP.2018.2848911).
[27] K.Y. Kapusuz, *et al.*: "Polarization reconfigurable air-filled substrate integrated waveguide cavity-backed slot antenna," IEEE Access **7** (2019) 102628 (DOI: 10.1109/ACCESS.2019.2926809).
[28] A. Ghosh and K. Mandal: "High gain and wideband substrate integrated waveguide based H-plane horn antenna," AEU-Int. J. Electron. Commun. **105** (2019) 85 (DOI: 10.1016/j.aeue.2019.04.005).
[29] S. Ahmadi: *5G NR: Architecture, Technology, Implementation, and Operation of 3GPP New Radio Standards* (Academic Press, 2019).
[30] C.A. Balanis: *Antenna Theory: Analysis and Design* (John Wiley & Sons, 2016).